AGU PUBLICATIONS

Geophysical Research Letters

RESEARCH LETTER
10.1002/2015GL063589

Key Points:
- Models of InSAR deformation at Sabancaya show tectonic activity
- Most earthquakes are tectonic, but some may be related to the magmatic system
- Seismicity increased in June 2014 and culminated in phreatic eruption

Supporting Information:
- Supporting Information 1
- Figure S1
- Figure S2
- Figure S3
- Figure S4
- Figure S5
- Figure S6
- Figure S7
- Figure S8
- Figure S9
- Figure S10
- Figure S11

Correspondence to:
J. A. Jay,
jayj@si.edu

Citation:
Jay, J. A., F. J. Delgado, J. L. Torres, M. E. Pritchard, O. Macedo, and V. Aguilar (2015), Deformation and seismicity near Sabancaya volcano, southern Peru, from 2002 to 2015, *Geophys. Res. Lett.*, *42*, doi:10.1002/2015GL063589.

Received 21 FEB 2015
Accepted 16 MAR 2015
Accepted article online 19 MAR 2015

Deformation and seismicity near Sabancaya volcano, southern Peru, from 2002 to 2015

Jennifer A. Jay[1,2], Francisco J. Delgado[1], José Luis Torres[3], Matthew E. Pritchard[1], Orlando Macedo[3], and Victor Aguilar[4]

[1]Department of Earth and Atmospheric Sciences, Cornell University, Ithaca, New York, USA, [2]Smithsonian Institution, Washington, District of Columbia, USA, [3]Observatorio Vulcanológico del Sur, Instituto Geofísico del Perú, Arequipa, Peru, [4]Instituto Geofísico de la Universidad Nacional de San Agustín, Arequipa, Peru

Abstract We use interferometric synthetic aperture radar (InSAR) and local seismic data to investigate the cause of earthquake sequences near Sabancaya volcano in southern Peru from 2002 to 2014, with a particular focus on events leading up to the August 2014 phreatic eruption. InSAR-observed deformation associated with earthquake swarms in late 2002, February 2013, and July 2013 is modeled by fault slip, with no need for magmatic sources to explain the deformation. The majority of the seismicity is an expression of the regional tectonic system, which is characterized by E-W trending normal faults, but a link to the magmatic system is possible. The M_w 5.9 earthquake on 17 July 2013 occurred on a previously unmapped normal fault that continued to deform in the months following the earthquake. An increase in long period and hybrid seismicity and changes in fumarolic emissions in 2013–2014 culminating in the August 2014 eruption indicates the involvement of both tectonic and magmatic systems.

1. Introduction and Background

Volcano-tectonic (VT) seismicity is a common occurrence at active volcanoes and generally indicates shear failure in response to the local magmatic stress regime [e.g., *Lahr et al.*, 1994; *Roman and Cashman*, 2006]. The magnitudes of VT earthquakes are generally small and very rarely exceed M_w 4.5 [*Zobin*, 2001], making it difficult to detect these earthquakes without a local seismic network. Sabancaya volcano in southern Peru is an example where multiple teleseismically recorded shallow swarms with $M_w > 4.5$ have occurred between 2002 and 2013. Though these swarms were not obviously related to the volcanic system and were larger in magnitude than most typical VT earthquakes, their proximity to Sabancaya (within 25 km of the summit) raises the question of whether the seismicity was magmatically driven or purely tectonic in nature.

Sabancaya is the youngest of three edifices in a volcanic complex that includes Hualca Hualca to the north and Ampato to the south. InSAR (interferometric synthetic aperture radar) studies show that between 1992 and 1997, a circular region ~50 km in diameter centered near Hualca Hualca experienced uplift of about 2 cm/yr in the center of deformation [*Pritchard and Simons*, 2002; *Pritchard and Simons*, 2004] (green dashed circle in Figure 1b). Shallow crustal earthquakes in the region around Sabancaya are historically infrequent in global catalogs, however, since early 2013 seismicity has greatly increased—the U.S. Geological Survey (USGS) catalog reports nine earthquakes in 2013 within 50 km of Sabancaya and with depths less than 30 km, while only seven earthquakes total were reported between 1973 and 2012. Several $M_w > 5$ earthquakes in the 1990s may have been related to the 1990–1998 eruption of Sabancaya [*Rodríguez and Uribe*, 1994; *Antayhua et al.*, 2001, 2002].

Sabancaya volcano is a dacite to andesite stratovolcano located in the Andean Central Volcanic Zone of southern Peru (Figure 1). The most recent eruption of Sabancaya spanned 1990–1998, following about 200 years of dormancy [*Gerbe and Thouret*, 2004]. The volcano is surrounded by an extensive system of active faults and lineaments (Figure 1c)—the Huambo-Cabanaconde Fault Zone to the northwest, which is composed of the Trigal and Solarpampa normal faults and minor subparallel faults; the Ichupampa normal fault to the northeast; the Pampa Sepina fault zone and Sepina lineament to the east; and the Huanca normal fault to the southwest [*Sebrier et al.*, 1985; *Mering et al.*, 1996; *Huamán-Rodrigo et al.*, 1993; *Macharé et al.*, 2003].

In this paper, we use InSAR along with local and global earthquake catalogs to investigate the origin of these earthquake swarms and determine whether they were related to magmatic activity.

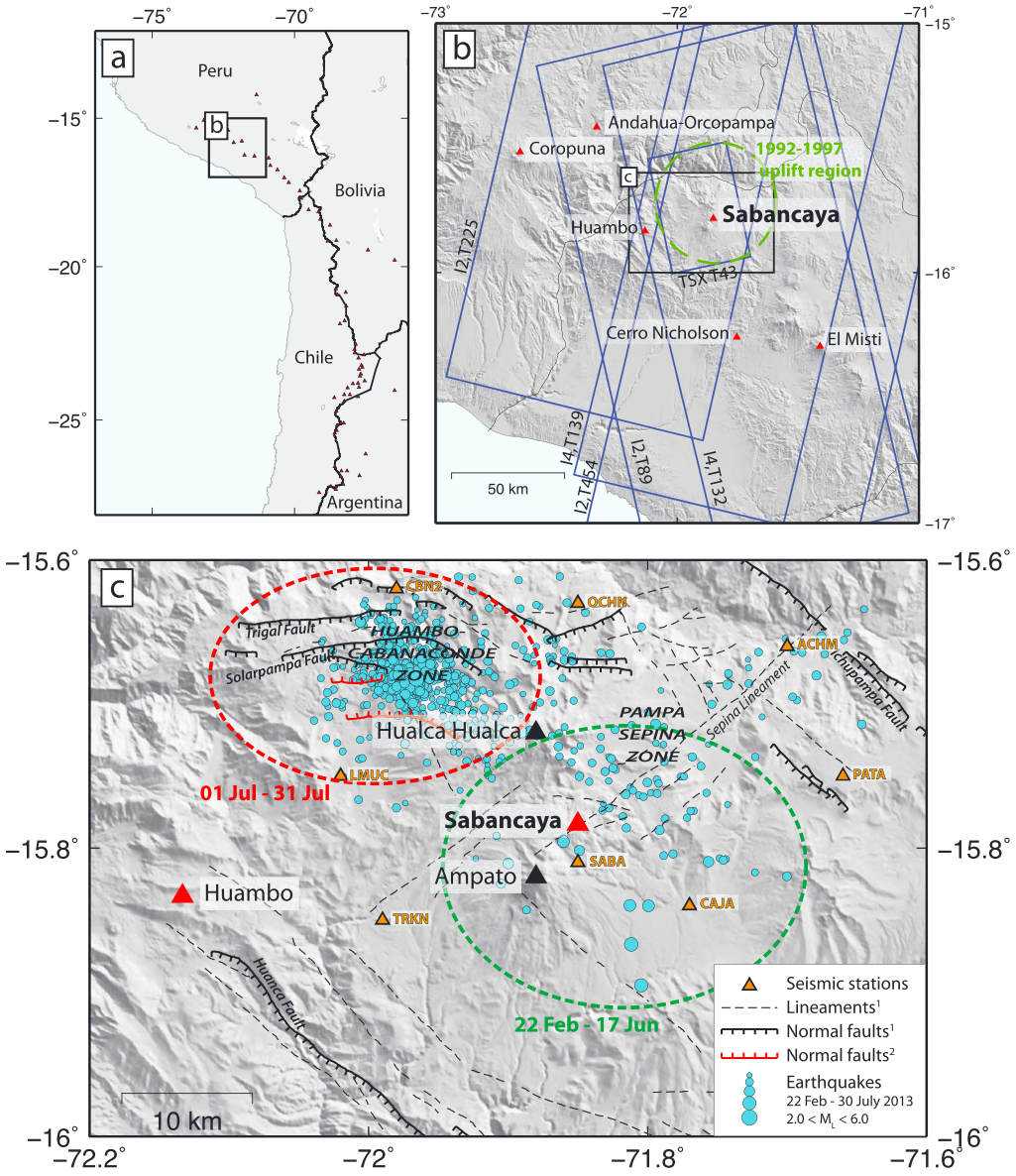

Figure 1. (a) Overview map of the Andean Central Volcanic Zone (CVZ) of Peru, Bolivia, Chile, and Argentina. Black rectangle indicates region depicted in Figure 1b. (b) Map of southern Peru showing the location of Sabancaya volcano. Blue rectangles indicate satellite tracks. Green circle indicates the extent of the region that experienced uplift between 1992 and 1997. Red triangles show the locations of Holocene volcanoes from the Smithsonian Institution Volcanoes of the World database [*Siebert and Simkin,* 2002-2015]. (c) Zoom-in map of the Sabancaya region. VT seismicity between 22 February and 30 July 2013 is shown as blue circles. Colored regions indicate temporal migration of seismicity from the south during 22 February to 17 June 2013 (green) to the northwest during 1–31 July 2013 (red). The superscript 1 indicates faults and lineaments from *Antayhua et al.* [2002], and the superscript 2 indicates faults that ruptured in July 2013 based on InSAR deformation (this study).

2. Methods

2.1. InSAR

We use all available SAR data from the European Space Agency's (ESA) ERS-1, ERS-2, and Envisat C-band (5.6 cm wavelength) satellites from 1995 to 2010. Due to the recent earthquake activity at Sabancaya, we also requested data acquisitions from the German Aerospace Center's (DLR) TerraSAR-X X-band (3.1 cm wavelength) satellite between 14 January 2012 and 18 January 2015 to image deformation that spans the time period of heightened seismicity. We process data from the satellite tracks displayed in Figure 1 and

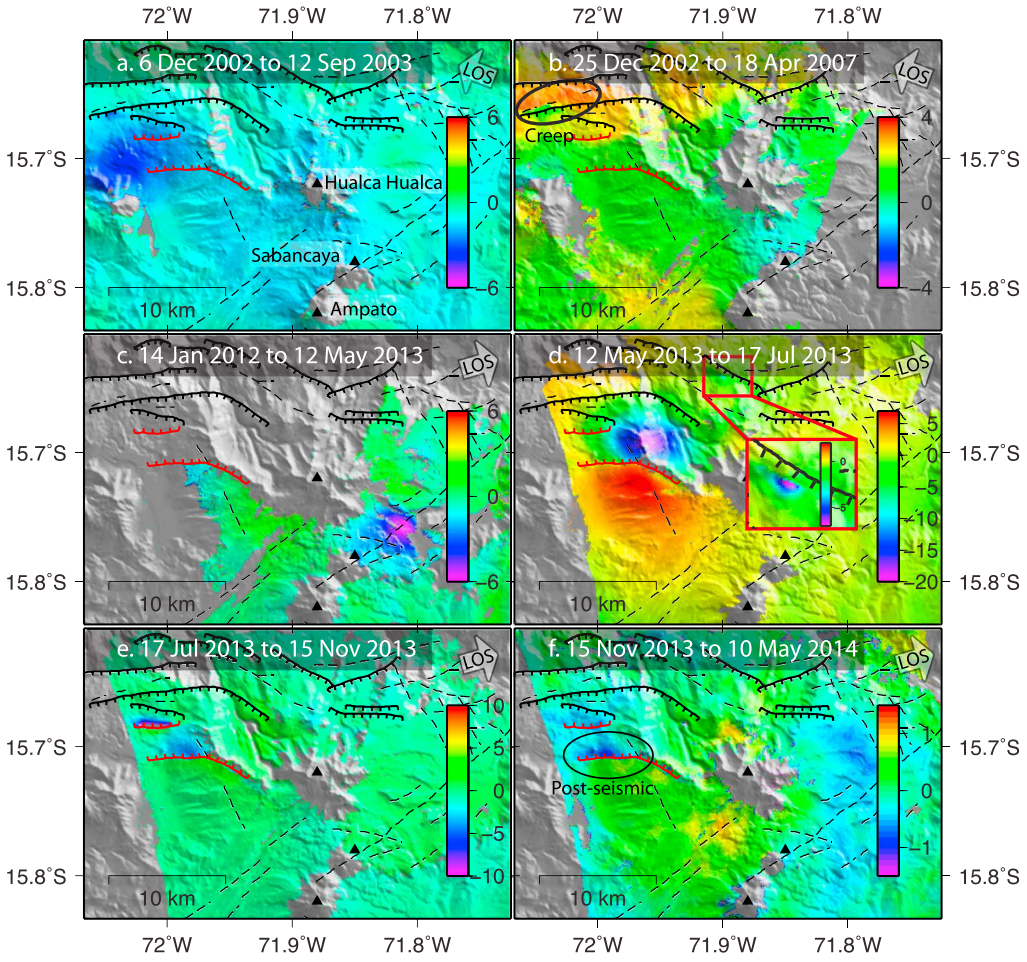

Figure 2. Interferograms showing line of sight deformation (cm) at Sabancaya volcano between 2002 and 2013. (a) ERS interferogram from track 454 showing subsidence related to the M_w 5.3 earthquake on 13 December 2002; (b) Envisat interferogram from track 225 beam 2 showing possible creep across the Solarpampa fault; (c) TerraSAR-X interferogram showing deformation related to the earthquake swarm in late February 2013; (d) TerraSAR-X interferogram showing deformation related to the M_w 5.9 earthquake on 17 July 2013 and inset showing deformation related to another earthquake of smaller magnitude; (e) TerraSAR-X interferogram showing deformation related to aftershock activity following the 17 July earthquake; (f) TerraSAR-X interferogram showing postseismic deformation. © DLR 2013, 2014.

listed in Table S1 in the supporting information using the ROI_PAC software [*Rosen et al.*, 2004]. Deformation is modeled by slip on a fault plane embedded in a homogeneous elastic half-space [*Okada*, 1992], and best fit parameters are inferred using a Neighborhood Algorithm [*Sambridge*, 1999] after interferogram downsampling [*Lohman and Simons*, 2005].

2.2. Seismicity

Three strong shallow earthquakes (depth $<$ 8 km) with magnitudes 4.6, 5.2, and 5.0 M_L occurred on 22 February 2013 at distances between 2 and 12 km to the south and SE of Sabancaya volcano (see section 3.2). A few hours later, the Observatorio Vulcanológico del Sur, Instituto Geofísico del Perú set up a network of nine temporary seismic stations around the volcano at distances between 3 and 22 km away from the crater (Figure 1c). Three stations (SABA, CAJA, and PATA) were equipped with CMG40T sensors (0.033–50 Hz) and RefTek recorders, one station (ACHM) had a Lennartz-3Dlite sensor (1 Hz, 3C) coupled with a Guralp CMG-DM24 digitizer, and the remaining five sites (CBN2, TRKN, LMUC, OCHN, and SLL2) operated with Guralp CMG-6TD broadband compact stations (0.033–100 Hz). Between 23 February and 29 July 2013, 1328 long period (LP) or low-frequency earthquakes were registered, as well as 13,485 volcano-tectonic (VT) or high-frequency earthquakes. Of the VT events, 894 were clearly recorded by at least seven stations and were located using the HYPOELLIPSE computer

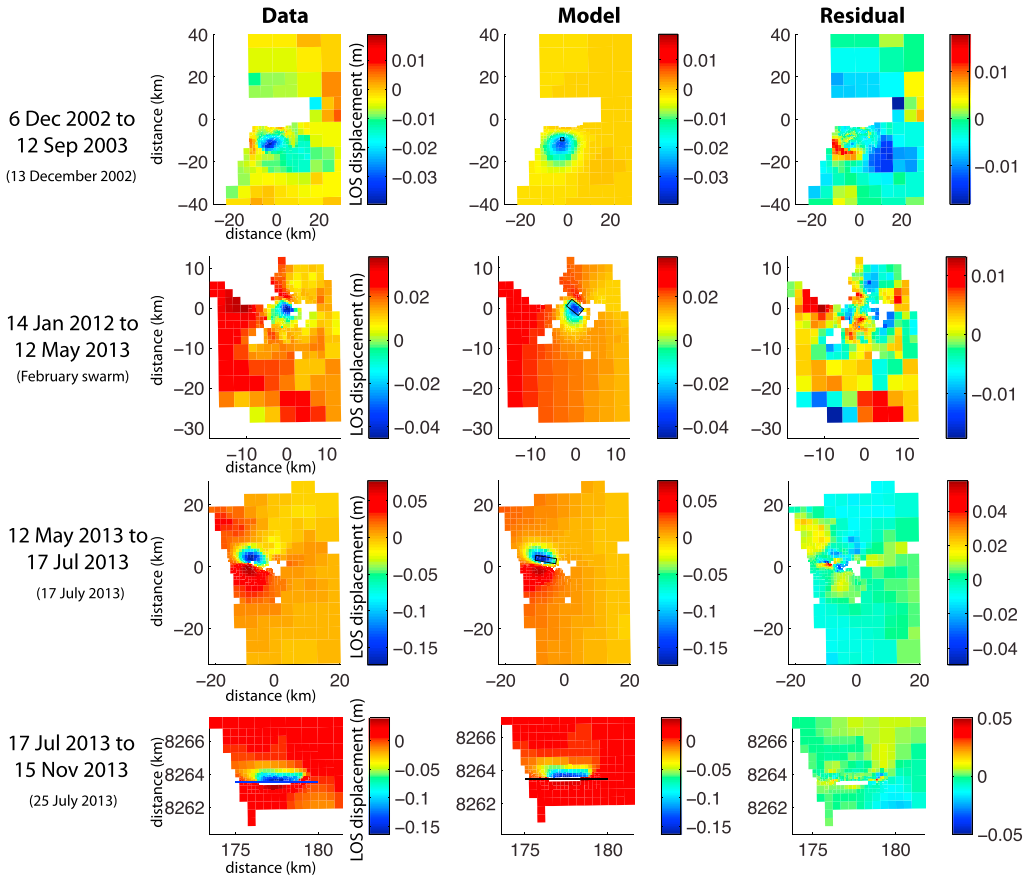

Figure 3. Sabancaya earthquake modeling results for (top to bottom) the M_w 5.3 13 December 2002 earthquake, the February 2013 earthquake swarm, the M_w 5.9 17 July 2013 earthquake, and the 25 July 2013 earthquake.

program [*Lahr*, 1999]. Furthermore, using the FOCMEC [*Snoke et al.*, 1984] and HASH [*Hardebeck and Shearer*, 2002] programs, the focal mechanisms of 22 VT events with clear *P* wave arrivals were determined. Earthquakes that occurred after 29 July 2013 were recorded but not analyzed due to operational problems with the seismic network.

3. Results and Modeling

3.1. December 2002

An Envisat interferogram spanning 6 December 2002 to 12 September 2003 shows a region of subsidence located about 20 km NW of the summit of Sabancaya with a maximum displacement of about 5 cm in the satellite line of sight (LOS) (Figure 2a). This lobe of subsidence is located just south of the Solarpampa fault, an east striking normal fault 14 km in length with a dip of 65° [*Macharé et al.*, 2003] and a principal fault of the Huambo-Cabanaconde system (Figure 1c). The deformation is likely related to a swarm of earthquakes that occurred on and near this fault on 13 December 2002, the largest of which was M_w 5.3.

InSAR modeling results give a cumulative moment magnitude of 5.8 and a depth of 12.2 km for this earthquake swarm (Figure 3). The focal mechanism and depth derived from InSAR are similar to that of the Global centroid moment tensor (CMT) catalog, but the dip from InSAR of 68° is significantly steeper than the dip from Global CMT of 46°. The dip from InSAR modeling more closely agrees with field measurements of the Solarpampa fault, which indicate a dip of 65° [*Macharé et al.*, 2003]. The magnitude from InSAR modeling (M_w 5.8) is larger than the CMT magnitude (M_w 5.3); this can partially be reconciled by the fact that the there were three additional $M_w > 4$ earthquakes that occurred on 13 December 2002 in the same region with reported depths of 33 km (USGS catalog). However, the scalar sum of the seismic moments from all

Date		InSAR	GCMT	Local
13 Dec 2002	Depth (km)	12.2	15.0	N/A
	Mw	5.8	5.3	N/A
	Focal Mechanism			N/A
22-23 Feb 2013	Depth (km)	4.1	27.5, 20.4, 15.9, N/A	5, 8, 7, 5
	Mw	5.5	5.0, 5.3, 5.4, N/A	4.7, 5.2, 4.9, 4.6
	Focal Mechanism		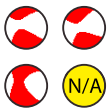	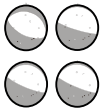
17 Jul 2013	Depth (km)	3.5	12	8
	Mw	5.8	6.0	5.9
	Focal Mechanism			
25 Jul 2013	Depth (km)	1.0	19.2	3.0
	Mw	5.0	4.8	3.6
	Focal Mechanism	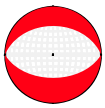	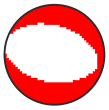	N/A

Figure 4. Comparison of depths, magnitudes, and focal mechanisms for the four Sabancaya earthquake sequences calculated by InSAR modeling, the Global CMT, and local seismic networks. InSAR modeling for the February swarm calculates one solution for all swarm events since the interferogram spans the duration of the swarm.

cataloged earthquakes in the swarm does not add up to M_w 5.8. Based on evidence of postseismic deformation between 2002 and 2007 (Figure 2b), we suggest that additional slip may have occurred aseismically on the same fault during the 9 months spanned by the coseismic interferogram. The earthquake was similar in location and focal mechanism to the 1998 M_L 5.2 Cabanaconde earthquake, which was thought to be purely a result of regional extension and unrelated to the Sabancaya volcanic system [*Antayhua et al.*, 2002]. Only one interferogram spans the 1998 Cabanaconde earthquake, but any deformation that may have been caused by the earthquake is not apparent due to atmospheric contamination (supporting information).

3.2. February 2013

An earthquake swarm occurred near Sabancaya on 22–23 February 2013, and the magnitudes of the largest four earthquakes ranged from M_w 4.6 to 5.2. These four earthquakes were all shallow, with depths $<$ 8 km. A

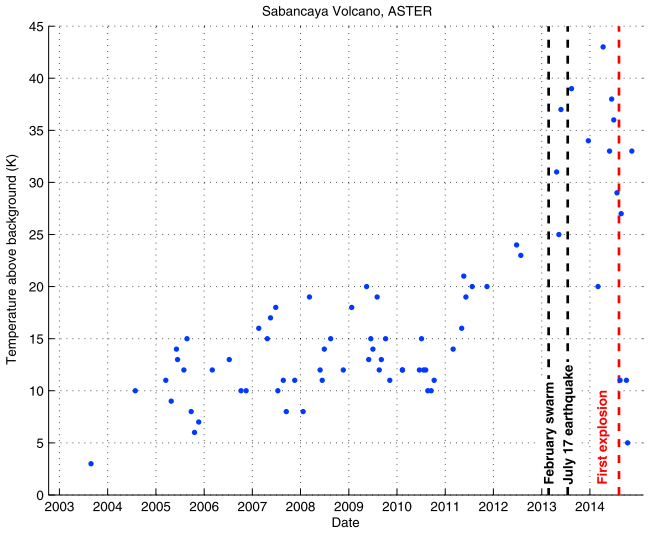

Figure 5. Fumarole temperature time series from ASTER satellite thermal infrared data (90 m resolution). The temperature above background is determined by differencing the temperature of the hottest pixel with the average temperature of surrounding cold pixels.

TerraSAR-X interferogram that spans 14 January 2012 to 12 May 2013 shows a region of subsidence of 6 cm maximum LOS in the region of the swarm (Figure 2c), about 6 km NE of the summit of Sabancaya. Modeling of this interferogram gives a cumulative moment magnitude of M_w 5.5 and a depth of 4.1 km on a SE striking oblique normal fault dipping 69° to the SW (Figure 3). Focal mechanisms derived from the InSAR modeling are similar to the Global CMT and local network focal mechanisms (Figure 4). However, depths calculated by the Global CMT are more than 10 km deeper than InSAR and local depths, a common discrepancy [e.g., *Weston et al.*, 2011].

We also observe increased fumarolic emissions of water vapor and magmatic gas during this time period [*Global Volcanism Program*, 2013]. Using satellite thermal infrared data from the Advanced Spaceborne Thermal Emission and Reflection Radiometer (ASTER) instrument (90 m resolution) and the methods employed by *Jay et al.* [2013], we find that the fumarole temperature at the summit increased from an average of 13°C above background from 2003 to 2012 to an average of 33°C above background in 2013 (Figure 5).

3.3. July to November 2013

From 15 to 25 July 2013, the summit seismic station (SABA, located 3 km south of the crater) recorded a strong increase in the number of hybrid earthquakes. On 17 July 2013, following about 2 days of precursory M_L 3–4 seismicity, a M_w 5.9 earthquake occurred at 7 km depth about 15 km NW of Sabancaya. A TerraSAR-X interferogram spanning 12 May 2013 to 17 July 2013 shows a maximum of 16 cm subsidence in the LOS and 6 cm uplift in the LOS (Figure 2d). Modeling of the 12 May to 17 July 2013 interferogram gives a moment magnitude of M_w 5.8 and a depth of 3.5 km (Figure 4) on a W striking normal fault dipping 62° to the north. The InSAR focal mechanism is consistent with the focal mechanism calculated from the local seismic network (Figure 4). In addition to the deformation from the large 17 July earthquake, the interferogram also contains a smaller deformation signal located ~10 km NNW of Hualca Hualca (Figure 2d, inset) with 6 cm LOS subsidence. We believe that this signal is related to an earthquake that occurred in the Huambo-Cabanaconde zone on a nearby mapped normal fault, which displays the appropriate strike to have produced the observed deformation.

An interferogram spanning 17 July 2013 to 15 November 2013 shows at least two distinct areas of deformation in the same region as the 17 July 2013 earthquake, presumably related to aftershock activity and postseismic deformation (Figure 2e). A simple distributed slip model with a uniform rake of −90° was considered to model the EW normal fault earthquake of 25 July which was recorded by the Global CMT catalog (supporting information). The slip model yields a moment magnitude of 5.0, slightly larger than the M_w 4.8 reported by the Global CMT catalog (Figure 4).

The 17 July 2013 earthquake and aftershocks occurred on previously unmapped faults, south of the Huambo-Cabanaconde system. The focal mechanisms and deformation patterns are consistent with the N-S extension that is characteristic of the Huambo-Cabanaconde system, but the faults differ in that they dip to the north rather than to the south.

3.4. November 2013 to May 2014

A TerraSAR-X interferogram spanning 15 November 2013 to 10 May 2014 shows motion across the western part of the same fault that ruptured during the 17 July 2013 earthquake (Figure 2f). We interpret this aseismic

motion to be postseismic deformation caused by afterslip, or continued creep on the fault. This idea is supported by the fact that the sense of motion is the same as the 17 July earthquake—subsidence of the hanging wall to the north and uplift of the footwall to the south. The small number of TerraSAR-X acquisitions does not allow us to determine whether the rate of postseismic deformation decays with time.

3.5. August 2014

Sabancaya experienced two phreatic explosions in August 2014. The first occurred on 9 August and lasted 55 s with coda duration magnitude M_d 2.2, and the second occurred on 25 August and lasted 82 s with M_d 2.7. Rates of VT, LP, and hybrid seismicity increased significantly in the week leading up to the first explosion (supporting information). In the days following the first explosion, LP seismicity remained elevated but hybrid seismicity diminished. A regional tectonic earthquake near the coast with local magnitude 5.7 occurred on 25 August, 11 h prior to the second explosion. A small confined explosion occurred on 11 November 2014. Interferograms spanning 10 May to 17 August 2014, 17 August to 2 November 2014, and 2 November 2014 to 18 January 2015 show no measurable deformation (supporting information).

4. Discussion and Conclusions

InSAR modeling shows that deformation in late 2002, February 2013, and July 2013 can be fully accounted for by faulting; in other words, no volcanic sources (i.e., Mogi, dyke, and sill) are required in the modeling. The local seismic catalog of all VT earthquakes from 22 February to 30 July 2013 has a *b* value of 0.95 (supporting information), a typical value for tectonic areas but lower than in many volcanic areas where fluids are involved [*McNutt*, 2005]. The locations and extensional nature of these events strongly suggest that they are associated with the regional tectonics. Normal faulting and extension is common at high elevations such as the Andes of southern Peru and is often caused by gravitational and buoyancy forces exerted by high topography and thick crustal roots [e.g., *Dalmayrac and Molnar*, 1981]. Such forces may contribute to the development of the extensive system of faults in the Sabancaya region (Figure 1c).

While direct involvement of magma is not apparent in the surface deformation and *b* value analysis, other evidence indicates activation of the magmatic system beginning in 2013 and culminating in the 2014 eruption. First, the earthquake sequence of February 2013 fits into the category of a swarm, with many events of similar magnitude closely clustered in space and time. Models for swarm generation generally involve initiation of activity by magmatic or other fluid processes [e.g., *Hill*, 1997]. Second, the occurrence of hybrid and LP events is indicative of fluid processes, as the proposed mechanisms for generation of such events typically involve pressure fluctuations in a fluid [e.g., *Chouet*, 1996]. Third, the change in fumarolic emissions (increased output and higher temperatures) beginning in February 2013 is a manifestation of changes in the magmatic and/or hydrothermal system. Thus, although the earthquake sequences of February and July 2013 were an expression of the regional tectonic regime, it is likely that they were also linked to the motions of magmatic and/or hydrothermal fluids that ultimately led to the phreatic eruption of August 2014. Perhaps the extension caused by the earthquakes created a favorable pressure gradient for magma to rise through the shallow crust or fluid movement helped trigger the earthquakes. However, if magmatic activity is at play, it is not apparent in the surface deformation observations within the detection limits of our InSAR data.

The proximity of the faults involved in the 2013 earthquakes raises the question of whether the later earthquakes were triggered by earlier ones. Static Coulomb stress models suggest that the 22 February earthquake swarm did not trigger the 17 July earthquake, as the magnitude of stress change at the epicenter of the 17 July earthquake was insignificant. Likewise, an increase in the Coulomb stress imposed by the 17 July earthquake could not have triggered the 25 July earthquake (supporting information).

Though large earthquakes are rare in volcanic settings, such events have occurred at several volcanoes. Ticsani volcano in Peru (175 km SE of Sabancaya) experienced an earthquake swarm but no subsequent eruptive activity [*Holtkamp et al.*, 2011; *Jay*, 2014]. Between 25 July and 20 October 2005, 31 earthquakes occurred within 50 km of Ticsani with depths less than 50 km and magnitudes ranging from M_w 4.0 to 5.3 [*Jay*, 2014]. In addition, Table 2 of *McNutt* [1996] lists 26 other large $M_{max} > 4.5$ earthquakes near volcanoes. Of these, only three occurred at arc volcanoes and not during eruption—Asama, Aso, and Miyakejima volcanoes in Japan. In all three cases, earthquake swarms lasting several days were followed by eruption 3 to 10 months later [*Abe*, 1979; *Kubotera and Mitsunami*, 1980; *Siebert and Simkin*, 2002-2015]. Similarly, the first explosion at

Sabancaya occurred more than 1 year after the large M_w 5.9 earthquake. These cases demonstrate that, though rare, large teleseismically recorded earthquakes do occur near volcanoes, and the time lag between earthquake and eruption can exceed 1 year.

In summary, InSAR data at Sabancaya reveals tectonic deformation while seismic data (particularly earthquake swarms, hybrid, and LP events) indicates magmatic and/or hydrothermal activity. Deformation observed by InSAR is caused by fault slip on extensional structures; this is consistent with field studies that show that recent and active deformation in the region results from normal faulting on faults whose kinematics show N-S extension. Though no magmatically driven ground deformation was observed prior to eruption, local seismicity and fumarole emissions show that the magmatic system was activated as early as February 2013, more than a year before the August 2014 explosions. Sabancaya is an example of a volcano that is very seismically active but has not yet shown signs of magmatic deformation within a year before an eruption.

Acknowledgments

Partial support from NASA Earth Science program grant NNX12AM24G. The French Institut de recherche pour le développement (IRD) supplied five Guralp seismic stations which helped with the success of the seismic monitoring. The seismic study was financed by the PP 068, Meta 7 "Vigilancia Geofísica de Volcanes" of the Instituto Geofísico del Perú (IGP) Área de Vulcanología. We thank H. Tavera for the review of focal mechanism calculations and R. Machacca, R. Chijcheapaza, and A. Ramos for their help in the field. We also thank Scott Henderson for assistance with InSAR data processing. TerraSAR-X data are available through agreement with the German Aerospace Center (DLR) and the Committee on Earth Observation Satellites Disaster Risk Management Volcano Pilot Observation Project, and ERS/Envisat data are available through the European Space Agency (ESA) Category 1 proposal 3194. ASTER data are provided by NASA Land Processes Distributed Active Archive Center (LP DAAC). Finally, we thank Paul Lundgren, Mike Poland, and an anonymous reviewer for their extremely helpful comments.

The Editor thanks Paul Lundgren and an anonymous reviewer for their assistance in evaluating this paper.

References

Abe, K. (1979), Magnitudes of major volcanic earthquakes of Japan 1901 to 1925, *J. Fac. Sci., Hokkaido Univ., Ser. 7*, *6*(1), 201–212.

Antayhua, Y., H. Tavera, and I. Bernal (2001), Analisis de la actividad sismica en la region del volcán Sabancaya (Arequipa), *Bol. Soc. Geol. Peru*, *92*, 79–88.

Antayhua, Y., H. Tavera, I. Bernal, H. Palza, and V. Aguilar (2002), Localizacion hipocentral y caracteristicas de la fuente de los sismos de Maca (1991), Sepina (1992) y Cabanaconde (1998), Región del Volcán Sabancaya (Arequipa), *Bol. Soc. Geol. Peru*, *93*, 63–72.

Chouet, B. (1996), Long-period volcano seismicity: Its source and use in eruption forecasting, *Nature*, *380*, 309–316.

Dalmayrac, B., and P. Molnar (1981), Parallel thrust and normal faulting in Peru and constraints on the state of stress, *Earth Planet. Sci. Lett.*, *55*, 473–481.

Gerbe, M.-C., and J.-C. Thouret (2004), Role of magma mixing in the petrogenesis of tephra erupted during the 1990–98 explosive activity of Nevado Sabancaya, southern Peru, *Bull. Volcanol.*, *66*(6), 541–561, doi:10.1007/s00445-004-0340-3.

Global Volcanism Program (2013), Report on Sabancaya (Peru), in *Bulletin of the Global Volcanism Network*, vol. 38, edited by R. Wunderman, Smithsonian Institution, doi:10.5479/si.GVP.BGVN201302-354006.

Hardebeck, J. L., and P. M. Shearer (2002), A new method for determining first-motion focal mechanisms, *Bull. Seismol. Soc. Am.*, *92*, 2264–2276.

Hill, D. (1977), A model for earthquake swarms, *J. Geophys. Res.*, *82*(8), 1347–1352, doi:10.1029/JB082i008p01347.

Holtkamp, S. G., M. E. Pritchard, and R. B. Lohman (2011), Earthquake swarms in South America, *Geophys. J. Int.*, *187*(1), 128–146, doi:10.1111/j.1365-246X.2011.05137.x.

Huamán-Rodrigo, D., J. Chorowicz, B. Deffontaines, R. Guillande, and J.-P. Rudant (1993), Cadre structural et risques geologiques etudies a l'aide de l'imagerie spatiale: La región du Colca (Andes du sud Perou), *Bull. Soc. Geol. Fr.*, *164*(6), 807–818.

Jay, J. A. (2014), A geophysical survey of active volcanism in the central and southern Andes, Cornell Univ.

Jay, J. A., M. Welch, M. E. Pritchard, P. J. Mares, M. E. Mnich, A. K. Melkonian, F. Aguilera, J. A. Naranjo, M. Sunagua, and J. Clavero (2013), Volcanic hotspots of the central and southern Andes as seen from space by ASTER and MODVOLC between the years 2000 and 2010, *Geol. Soc. London Spec. Publ.*, *380*(1), 161–185, doi:10.1144/SP380.1.

Kubotera, A., and Mitsunami, T. (1980), An earthquake swarm in the northern part of the Aso caldera and migration of their foci, *Tectonophysics*, *70*, 223–236. [Available at http://www.sciencedirect.com/science/article/pii/0040195180902802.]

Lahr, J., B. Chouet, C. Stephens, J. Power, and R. Page (1994), Earthquake classification, location, and error analysis in a volcanic environment: Implications for the magmatic system of the 1989–1990 eruptions at Redoubt Volcano, Alaska, *J. Volcanol. Geotherm. Res.*, *62*, 137–151.

Lahr, J. C. (1999), HYPOELLIPSE: A computer program for determining local earthquake hypocentral parameters, magnitude, and first-motion pattern, *U.S. Geol. Surv. Open File Rep. 99-23*.

Lohman, R. B., and M. Simons (2005), Some thoughts on the use of InSAR data to constrain models of surface deformation: Noise structure and data downsampling, *Geochem. Geophys. Geosyst.*, *6*, Q01007, doi:10.1029/2004GC000841.

Macharé, J., C. H. Fenton, M. N. Machette, A. Lavenu, C. Costa, and R. L. Dart (2003), Database and map of Quaternary faults and folds in Perú and its offshore region, USGS open-file report 03-451.

McNutt, S. R. (1996), Seismic monitoring and eruption forecasting of volcanoes: A review of the state-of-the-art and case histories, in *Monitoring and Mitigation of Volcano Hazards*, edited by R. Scarpa and R. I. Tilling, pp. 99–146, Springer, Berlin.

McNutt, S. R. (2005), Volcanic seismology, *Annu. Rev. Earth Planet. Sci.*, *33*(1), 461–491, doi:10.1146/annurev.earth.33.092203.122459.

Mering, C., D. Huaman-Rodrigo, J. Chorowicz, B. Deffontaines, and R. Guillande (1996), New data on the geodynamics of southern Peru from computerized analysis of SPOT and SAR ERS-1 images, *Tectonophysics*, *259*, 153–169.

Okada, Y. (1992), Internal deformation due to shear and tensile faults in a half-space, *Bull. Seismol. Soc. Am.*, *82*(2), 1018–1040.

Pritchard, M. E., and M. Simons (2002), A satellite geodetic survey of large-scale deformation of volcanic centres in the central Andes, *Nature*, *418*(6894), 167–71, doi:10.1038/nature00872.

Pritchard, M. E., and M. Simons (2004), An InSAR-based survey of volcanic deformation in the central Andes, *Geochem. Geophys. Geosyst.*, *5*, 1–42, doi:10.1029/2003GC000610.

Rodríguez, A., and M. Uribe (1994), Participación del Instituto Geofísico del Perú en relación con la reactivación del volcán Sabancaya, Provincia de Caylloma, Región Arequipa, Informe División de Sismología y Gravimetría, IGP-Arequipa, mayo 1994, 14 p.

Roman, D. C., and K. V. Cashman (2006), The origin of volcano-tectonic earthquake swarms, *Geology*, *34*(6), 457, doi:10.1130/G22269.1.

Rosen, P., S. Hensley, G. Peltzer, and M. Simons (2004), Updated repeat orbit interferometry package released, *Eos Trans. AGU*, *85*.

Sambridge, M. (1999), Geophysical inversion with a neighbourhood algorithm—I. Searching a parameter space, *Geophys. J. Int.*, *138*(2), 479–494, doi:10.1046/j.1365-246X.1999.00876.x.

Sebrier, M., J. L. Mercier, F. Megard, G. Laubacher, and E. Carey-Gailhardis (1985), Quaternary normal and reverse faulting and the state of stress in the central Andes of south Peru, *Tectonics*, *4*(7), 739–780, doi:10.1029/TC004i007p00739.

Siebert, L., and T. Simkin (2002-2015), Volcanoes of the world: An illustrated catalog of holocene volcanoes and their eruptions, in *Smithsonian Institution, Global Volcanism Program Digital Information Series*, GVP-3, Smithsonian Institution, Washington, D. C. [Available at www.volcano.si.edu.]

Snoke, J. A., J. W. Munsey, A. G. Teague, and G. A. Bollinger (1984), A program for focal mechanism determination by combined use of polarity and SV-P amplitude ratio data, *Earthquake Notes*, *55*(3), 15.

Weston, J., A. M. G. Ferreira, and G. J. Funning (2011), Global compilation of interferometric synthetic aperture radar earthquake source models: 1. Comparisons with seismic catalogs, *J. Geophys. Res.*, *116*, B08408, doi:10.1029/2010JB008131.

Zobin, V. M. (2001), Seismic hazard of volcanic activity, *J. Volcanol. Geotherm. Res.*, *112*, 1–14, doi:10.1016/S0377-0273(01)00230-X.